Prediction Experiments of Hurricane Gloria (1985) Using a Multiply Nested Movable Mesh Model

YOSHIO KURIHARA, MORRIS A. BENDER, ROBERT E. TULEYA AND REBECCA J. ROSS

Geophysical Fluid Dynamics Laboratory/NOAA, Princeton University, Princeton, New Jersey

(Manuscript received 5 March 1990, in final form 20 April 1990)

ABSTRACT

The prediction capability of the GFDL triply nested, movable mesh model, with finest grid resolution of 1/6 degree, was investigated using several case studies of Hurricane Gloria (1985) during the period that the storm approached and moved up the east coast of the United States. The initial conditions for these experiments were interpolated from an NMC T80 global analysis at 0000 UTC 25 September and 1200 UTC 22 September. The integrations starting from 0000 UTC 25 September were run 72 h, while those starting on 1200 UTC 22 September were run 132 h. The lateral boundary conditions were obtained from either an integration of the NMC T80 forecast model or the T80 global analysis, or were fixed to the initial value.

The model's predicted track of Gloria for each integration was compared against the best track determined by the National Hurricane Center (NHC). For the case starting from 0000 UTC 25 September using a forecasted boundary condition, the model successfully forecasted significant acceleration of the storm's movement after 48 h. The 72 h forecast error was about 191 km, compared to 480 km for the official track forecast made by the NHC.

To examine the model's skill in simulating the storm structure, distributions of the low level maximum wind and total storm rainfall during passage of the model storm are shown and compared with observed values. The model successfully reproduced many observed features such as the occurrence of strong winds well east of the storm center, with an abrupt decrease of the wind field along the coastline. When the storm track was accurately forecasted, the total storm rainfall amounts agreed well with the observed values. In both the model integration and observations, a significant structural change took place as the storm accelerated toward the north with little significant precipitation occurring south of the storm center and heavy precipitation spreading well north of the storm. It appears that the gross features of the structure of the storm's outer region resulted from the interaction of the vortex with its environment.

Sensitivity of the model forecast to the lateral boundary condition and the horizontal resolution was also investigated. The storm's track error was greatly affected after the boundary error propagated by advection to the storm region. The impact of the horizontal resolution on the forecast was such that the model with one degree resolution produced a fairly good track forecast up to 48 h, but failed to simulate some of the main structural features.

In the experiments starting from the 0000 UTC September 25 initial field, the interior storm structure did not develop, and the storm exhibited too large a radius of maximum wind throughout the integration. However, the integrations starting from 1200 UTC September 22 developed a more intense storm, with a more realistic radius of maximum wind. These differences were due to the spinup time necessary for the storm to develop in the model when starting from a coarse resolution global analysis which did not adequately resolve the fine structure of the storm interior. This indicates the importance of proper specification of the storm in the initial field.

1. Introduction

The purpose of this paper is to investigate the capability of the regional multiply nested movable mesh model constructed at the Geophysical Fluid Dynamics Laboratory, NOAA, (hereafter referred to as the MMM model), for the prediction of hurricane movement and structure. The cases studied are for Hurricane Gloria during the period that the storm approached and moved up the east coast of the United States. Hurricane Gloria of September, 1985, was one of the most widely reported weather events in recent decades. At its maximum intensity Gloria deepened to a minimum surface pressure of 919 mb, the lowest pressure measured by reconnaissance aircraft over the Atlantic Ocean up to that time (Case 1986). It exhibited considerably accelerated movement and marked asymmetric structure in the later period. These are the special features against which the model performance will be evaluated.

Accurate prediction of tropical cyclones requires accurate treatment of both the hurricane and its environment. To adequately resolve the fine scale of the hurricane, model resolution on the order of one sixth of a degree or less is required. Computational limita-

Corresponding author address: Dr. Yoshio Kurihara, NOAA/GFDL, P.O. Box 308, Princeton, NJ 08542.

tions make it impractical, however, to treat the entire model domain with such a fine resolution. On the other hand, the large scale synoptic flow field can adequately be treated by a much coarser model resolution. Thus a multiply-nested mesh model was constructed involving movable computational grids of variable resolution, with two-way interaction between these grids (Kurihara and Bender 1980, for more details). The usefulness of such a model has been demonstrated in various numerical studies using idealized conditions (e.g., Tuleya et al. 1984; Bender et al. 1987). In this study, the model was run with datasets obtained from real cases.

Obviously, the prediction of the hurricane's movement is a primary goal in the forecasting of the storm's future behavior. The increase of grid resolution may help to reduce the error in the track forecasting. In addition, with the development of very high resolution models, the forecast skill can hopefully be extended to include forecasts of storm intensity (e.g., minimum sea level pressure) and the distributions of other important quantities such as the total precipitation and low-level winds, assuming that the storm track has been reasonably forecasted. Such a conjecture is made on the assumption that the interaction between the storm vortex and the environment strongly influences the storm structure, e.g., the wind distribution. This type of interaction should be realistically represented in very high resolution models. Since the low-level mesoscale moisture convergence induces cumulus convection and the developed convective activities are more or less contained in the inertially stable region, the model precipitation will be realistic to the degree that the model wind field is realistic.

The forecast of the storm's intensity requires accurate specification of the initial conditions. The initial conditions for the experiments presented here were obtained from the uninitialized NMC (National Meteorological Center) T80 (Triangular truncation at wavenumber 80) global analysis, interpolated onto the appropriate grid resolutions of the MMM model and used directly. Since the hurricane vortex in the T80 analysis tended to be much too weak and unrealistically large, a "spinup" period was inevitable at the start of the integration of the MMM model. During this time it was anticipated that some of the storm's detailed structure and a more intense vortex would develop. Thus, a reasonable intensity prediction is not in the scope of the present study. Rather, emphasis will be placed on the simulation of the storm structure of the mature tropical cyclone which developed and interacted with the large scale field. The observed rainfall and wind measurements will be compared with those generated by the model. The innermost storm structure which was not resolved in the initial condition, may not properly develop during the integration with the MMM model. In future experiments with the MMM model, an appropriately determined vortex may be placed within the finest grid to more realistically represent the initial structure and intensity of the storm.

Although the continuing advancements in super computing capabilities have resulted in more realistic distributions of tropical cyclone structure with very high resolution global models (e.g., Krishnamurti et al. 1989; Krishnamurti and Oosterhof 1989), regional models are still necessary to resolve the finer scale of the storm structure as well as that of the surface conditions such as orography and sea surface temperature distribution. For regional models in general, proper treatment of the lateral boundary becomes very important and accurate boundary data has to be obtained from a host model. We will discuss the sensitivity of forecasting storm behavior to the type of lateral boundary datasets being used for the forcing.

A brief description of the model and experimental design will be presented in section 2. In section 3, results will be presented for the control experiment, a 72 hour forecast beginning on 0000 UTC 25 September. The results of the control will be compared with those using different lateral boundary datasets (section 4) and with those from coarse resolution experiments (section 5). Results from extended 132 h integrations will be shown in section 6. Finally a summary and concluding remarks are presented in section 7.

2. Description of model and experiments

a. Model description

The triply nested, movable grid system described previously by Kurihara and Bender (1980) was used for all integrations presented here. Specific model details have been outlined in previous publications (e.g., Tuleya et al. 1984; Bender et al. 1987). The model is a primitive equation model formulated in latitude, longitude, and sigma (σ, the pressure normalized by the surface value) coordinates, with the number of vertical levels expanded from 11 to 18. The vertical levels, summarized in Table 1, were identical to those used in the T80 analysis and T80 forecast model currently in use at NMC. The outermost domain stretched from 0° to 55°N in the meridional direction and from 95° to 40°W in the zonal direction. The grid system for each mesh is summarized in Table 2. The model physics include cumulus parameterization described by Kurihara (1973) with some modification (Kurihara and Bender 1980, appendix C), a Monin-Obukhov formulation for the surface flux calculation, and the Mellor and Yamada (1974) level-two turbulence closure scheme for the vertical diffusion, with a background diffusion coefficient added. The background coefficient decreases with height and is proportional to the square of sigma. The effect of radiative transfer is not treated explicitly. However, the zonal mean temperature was adjusted toward its initial value using a Newtonian-type damping.

TABLE 1. Summary of the vertical sigma levels for the MMM model.

k level	sigma
1	.0207469
2	.0739862
3	.1244004
4	.1745733
5	.2246687
6	.2747291
7	.3247711
8	.3748014
9	.4248250
10	.4974484
11	.5935378
12	.6881255
13	.7772229
14	.8563145
15	.9204018
16	.9604809
17	.9814907
18	.9949968

b. *Initial conditions*

The initial conditions were obtained from the uninitialized NMC T80 global analysis. The data were interpolated horizontally onto the regional model domain for each of the mesh resolutions. For the zonal and meridional components of the wind, a fifth-degree polynomial fit (Akima 1978) was used. This scheme resulted in a smooth fit of the wind components as well as the quantities of vorticity and divergence. For the moisture and mass fields, a simple bilinear interpolation was used in the horizontal. The distribution of surface height was obtained from the global topography dataset prepared by the U.S. Navy's Fleet Numerical Oceanography Center at Monterey, California. In this dataset the terrain height provided was the modal value for each $\frac{1}{6}°$ square area. The temperature, surface pressure and moisture fields over land were then adjusted for the differences between the NMC and the MMM topographical heights. The sea surface temperatures were set equal to the NMC analyzed values at the start of the integration and held fixed throughout each experiment. The land surface temperature at each point was set to the mean climatology for the month of September. The inner meshes were initially placed so that the storm was centered in the middle of the finest mesh at the start of the integration. (See Bender et al. 1987, section 2b and 2c, for more details on the treatment of topography and surface temperatures in the nested grid framework).

c. *Classification of experiments*

A summary of all the experiments performed is given in Table 3. Experiments were run from different initial times, using different lateral boundary conditions, and different horizontal resolutions. The number in each experiment name refers to the date of the start of the integration. The experiments starting on 0000 UTC 25 September were integrated for a three day period while those starting at 1200 UTC 22 September were integrated for an extended length of $5\frac{1}{2}$ days. According to Orlanski and Katzfey (1987), a numerical integration is defined as a *forecast* when the values at the lateral boundary are derived from a larger domain model forecast, and as a *simulation* when the lateral boundary is specified from a global analysis. For the experiments summarized here, the letter F at the end of the experiment name refers to those experiments run in forecast mode, with the data taken at 12 h intervals from an integration of the T80 model. Likewise, the letter A refers to those experiments run in simulation mode, with the boundary values taken every 12 h from the T80 analysis. The letter X refers to the integration where the boundary values were held fixed to the initial values throughout the integration. In all cases the specified lateral boundary values were linearly interpolated in time to hourly values. The model solution was then forced toward the nearest future hourly value at every time step. The model lateral boundary forcing was made with a scheme recently proposed by Kurihara et al. (1989). In their scheme all variables are damped toward a reference value, which is a combination of the actual value and the gradient of the value at the lateral boundary, defined from a host forecast model or global analysis. The amount of forcing is a function of the type of variable, the vertical sigma level, as well as the inflow angle of the wind at the boundary. Thus, a strong forcing was applied for inflow points and a

TABLE 2. Grid system of the triply nested mesh model used in each of the triply nested mesh experiments.

Mesh	Grid resolution (deg)	Domain size: Longitude (deg) (points)	Domain size: Latitude (deg) (points)	Time step (sec)
1	1	55 (55)	55 (55)	120
2	$\frac{1}{3}$	11 (33)	11 (33)	40
3	$\frac{1}{6}$	5 (30)	5 (30)	20

TABLE 3. Summary of numerical experiments discussed.

Experiment	Initial time	Type of boundary condition
G25F	0000 UTC 25 Sep	Forecasted
G25A	0000 UTC 25 Sep	Simulated
G25X	0000 UTC 25 Sep	Fixed
G25C (1°, one nest)	0000 UTC 25 Sep	Forecasted
G25T (1½°, one nest)	0000 UTC 25 Sep	Forecasted
G22F	1200 UTC 22 Sep	Forecasted
G22A	1200 UTC 22 Sep	Simulated

very weak forcing at outflow points. Finally, to test the impact of grid resolution, Expts. G25C and G25T were also integrated, with uniform resolutions everywhere of 1° and 1½°, respectively.

3. Results from experiment G25F

The disturbance which was to later strengthen into Hurricane Gloria, moved off the African coast on 15 September, becoming a tropical depression on 16 September, and strengthening to hurricane force on 22 September (Fig. 1). The system deepened 70 mb during the period from the 23rd to the 25th, reaching a maximum intensity of 919 mb around 0000 UTC 25 September. During the next 72 h Gloria approached the east coast of the United States, passing over the Outer Banks of North Carolina early on the 27th. In the subsequent 24 h the storm began to accelerate rapidly in a north-northeast direction, making landfall over central Long Island later in the day.

a. Track forecast

The initial field for the first experiment (Expt. G25F) was obtained from the T80 analysis on 0000 UTC 25 September, at approximately the time the hurricane reached its maximum intensity. The lowest sea level pressure, maximum lowest level winds, and radius of maximum wind in the T80 analysis at this time were 1001 mb, 27 m s^{-1}, and 470 km, respectively. This compares with the actual observed values of 920 mb, and 62 m s^{-1} for minimum sea level pressure and maximum low level winds and with a radius of maximum wind of about 18 km estimated from Fig. 5 of Franklin et al. (1988). The position error of the storm in the initial analysis was about 20 km. The model was integrated to 72 h with lateral boundary conditions supplied from an integration of the NMC T80 spectral model. The forecasted track (Expt. G25F) is shown in Fig. 2, with the observed track and the NHC (National Hurricane Center) 72 h forecasted track from 0000 UTC 25 September also plotted for comparison. The error statistics for each forecast are also summarized in Table 4, along with the forecast error for the NHC's statistical-dynamical model NHC83 (Neumann 1988), the CLIPER model, which is based on climatology and persistence (Neumann and Pelissier 1981), the NMC's MFM operational forecast model and the T80 forecast model. During the first 24 h, the storm moved erratically and significantly slower in the MMM forecast than observed. The initially slow movement was also a deficiency of the T80 forecast. Both forecasts may have suffered from the crude representation of the storm in the T80 analysis. By 48 h however, the MMM position was somewhat better than all five other forecasts. During the last 24 h of Expt. G25F, the model storm accelerated in a north-northeast direction, with a forecast error of 191 km after 72 h, significantly better than the NHC error of 480 km.

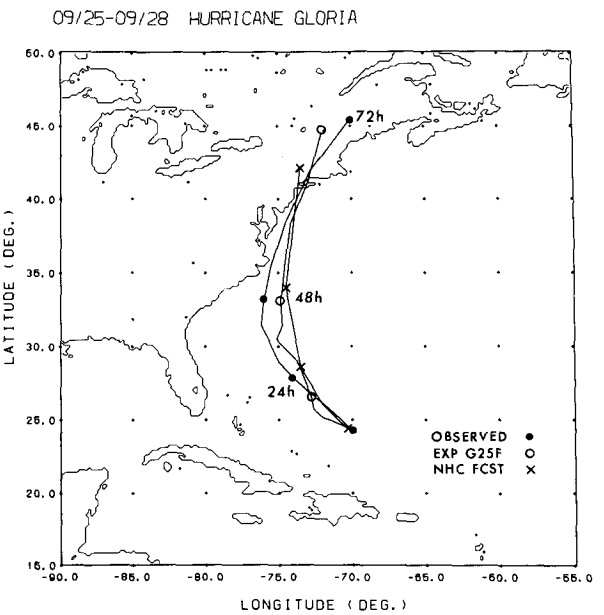

FIG. 2. The 72 h storm track from Expt. G25F, as well as the observed track (best track) and the National Hurricane Center (NHC) forecast track, made on 0000 UTC 25 September. The marks indicate the daily storm positions valid at 0000 UTC each day. The coastlines shown are those which are resolved by the finest mesh resolution (⅛°).

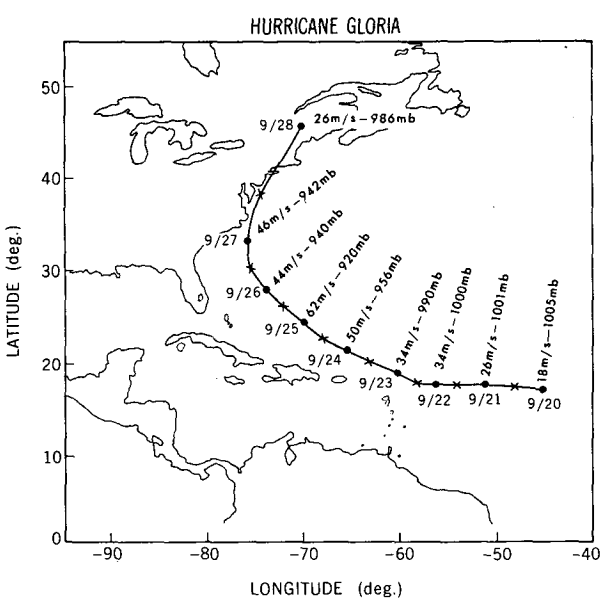

FIG. 1. Observed track (best track determined by the National Hurricane Center) of Hurricane Gloria during the period from 0000 UTC 20 September until 0000 UTC 28 September 1985. The storm's minimum sea level pressure (mb) and maximum low level wind (m s^{-1}) at 0000 UTC each day are shown. The large dots indicate the position of the storm at 0000 UTC and the ×'s indicate 1200 UTC storm positions.

TABLE 4. Summary of the forecast error (km) for various forecasts from initial time of 0000 UTC 25 September 1985.

Forecast time (h)	MMM (km)	NHC (km)	NHC83 (km)	CLIPER (km)	MFM (km)	T80 (km)
24	194	92	120	119	98	205
36	62	—	251	213	183	129
48	107	165	325	286	156	487
60	31	—	301	—	263	709
72	191	480	—	1023	—	—

In Fig. 3, the streamlines and isotachs of the deep layer mean wind, defined below, are presented for both the T80 analysis and the entire domain of Expt. G25F. At this time (60 h) Gloria was just east of southern Delaware, moving toward the north-northeast at about 17 m s^{-1}. The wind field plotted here is that of the vertically integrated large scale flow field with the disturbance field removed by application of a smoothing operator. (See the appendix for more details of the actual smoothing operator used). It is assumed that this will serve as a good approximation for the deep layer environmental flow field. Sanders and Burpee (1968) proposed the use of the deep layer mean wind in the barotropic track forecast of tropical cyclones. Neumann (1979) indicated that the tropical cyclone motion tends to be best correlated with the environmental flow field integrated through a deep layer. Indeed, from the tendency equation expressed in the form:

$$\partial p_*/\partial t = -\int_0^1 \mathbf{V}\, d\sigma \cdot \nabla p_* - p_* \int_0^1 \nabla \cdot \mathbf{V}\, d\sigma, \quad (3.1)$$

where p_* denotes the surface pressure and $\mathbf{V}$ the horizontal wind, it can be inferred that the deep layer mean wind is the steering flow for surface disturbances in general (the first term on the right hand side). This suggestion can be extended to the entire tropical cyclone system, due to the strong vertically coherent structure of tropical cyclones. Neumann's finding implies that the effect of the vertically integrated divergence, i.e., the second term on the right hand side of (3.1) usually tends to be relatively small, though it may not be negligible in some cases. Throughout the entire 72 h period of the present integration, the storm motion seemed to closely parallel the streamlines for the steering flows derived from both Expt. G25F and the T80 analysis. For example, the anticyclone observed over the Atlantic east of the United States was elongated toward the northwest at the start of the integration, resulting in movement in that direction at that time. However, as seen in Fig. 3, the orientation by 60 h had changed to the north-northeast, recurving the storm toward that direction. At this time, the mean flow near the storm center ($\sim$15 m s^{-1}) was about 2 m s^{-1} less than the observed storm speed of 17 m s^{-1}.

We clearly see that the deep layer mean wind field for Expt. G25F was quite similar to the mean wind field obtained from the T80 analysis. For example, the center position of the anti-cyclonic flow was very well forecast although its direction of elongation deviated slightly from the analysis, possibly contributing to the deviation of the storm track to the west of the best track during the last 12 hours of the forecast. The difference between the analysis and the forecast in the deep layer mean wind speed near the storm center was only about 2 m s^{-1}. As a whole the model successfully simulated the evolution of the large scale environmental flow field including the tropical regions where the vertical coherence of the wind is not strong. Therefore, the model was able to correctly capture the acceleration of the storm after 48 h, resulting in an excellent 72 h forecast of the track of Hurricane Gloria.

b. Forecast of low level winds and precipitation

An advantage of the MMM model's high resolution in the storm region is that we may expect a more accurate representation of important quantities such as wind and precipitation than has been possible previously with lower resolution simulations. Using a global model Heckley et al. (1987) obtained 48 h forecasted wind fields for Hurricane Elena just after landfall. Also, accumulated precipitation forecasts for Typhoon Tip (Dell'Osso and Bengtsson 1985) and forecasts of rainfall rates of Typhoon Irma (Iwasaki et al. 1987) have been obtained from integrations of limited area models, both with resolution of about 50 km. However, a more detailed structure of the storm fields was captured with the finer resolution of our model. In Fig. 4, we see the distribution of the maximum low level wind from Expt. G25F during passage of the storm up the east coast. The model storm produced strongest winds well east of the storm center, with a radius of maximum wind of about 210 km as the storm made landfall over Long Island. The large radius of maximum wind was in part due to the spin-up problem associated with the initial condition. However, the surface observations indicate that strong winds were indeed observed well east of the storm center during and after landfall. For example, although the storm center moved inland over western Connecticut, sustained winds of over 25 m s^{-1} were observed over a large section of the Massachusetts coastline with one reported wind speed in excess of hurricane force (Case 1986). We also note from Fig.

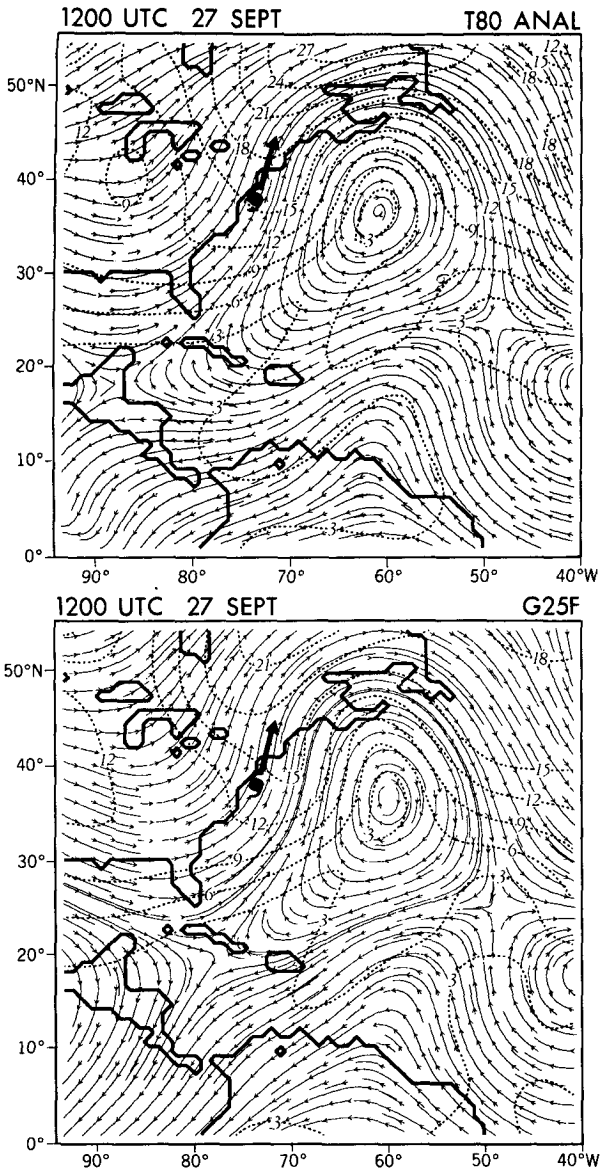

FIG. 3. The streamlines and isotachs (dashed line) of the deep layer mean wind at 1200 UTC 27 September, for the T80 analysis (top) and Expt. G25F (bottom). The coastline shown is that which is resolved by the 1° model resolution. The region shown is the entire integration domain used for each experiment. The observed storm position is indicated by the hurricane symbol with its direction of motion shown by the thick arrow.

4 the abrupt decrease of both the observed and modelled winds across the coastline, although the 20 m s^{-1} contour indicates that fairly strong winds still penetrated inland even after Gloria made landfall. Powell (1982) also showed an abrupt decrease in the wind speeds along the coast for Hurricane Frederic, as it made landfall. The forecasted wind speeds along the North Carolina coast were significantly less than observed values. This can partly be attributed to the long spin-up time of the model storm. Otherwise, there was good agreement between the observations and the model generated winds in Expt. G25F.

The distribution of the instantaneous precipitation during this time period is shown in Fig. 5. After 48 h, the southern eye wall of the model storm began to weaken and no significant precipitation was found south of the storm by hour 52. By this time the heaviest rainfall had spread well north and northwest of the storm center. The radar picture shown in Franklin et al. (1988, Fig. 8) indicated that little precipitation was occurring south of the storm center of Gloria as it moved over Cape Hatteras, with the heaviest rain falling north and west of the storm center. The mean diameter of the eye at this time was about 60 km, determined from the radar picture. It appears that the model did not capture the inner storm structure as the model's eyewall region, located at about 160 km radius from the storm center, was much too broad. However, the

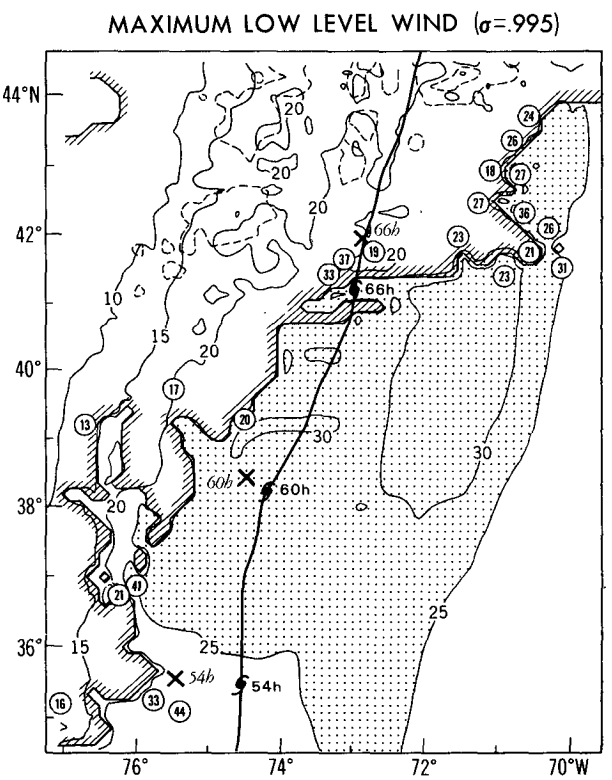

FIG. 4. Distribution of the predicted maximum low level (σ = 0.995) wind (m s^{-1}) during the passage of Hurricane Gloria, for Expt. G25F. Solid lines indicate the wind speeds at 5 m s^{-1} intervals, with areas above 25 m s^{-1} shaded. The numbers in circles are the observed values (m s^{-1}) of the maximum sustained winds. The forecasted storm track of the surface pressure center is shown by a thick solid line, with the storm position plotted at 6 h intervals. The observed storm positions at 6 h intervals are shown with ×'s. Heavy solid lines with short hatches indicate the shoreline, with the topographical heights (dashed lines) contoured at 500 m intervals. The topographical distribution and shoreline presented are those which are resolved by the finest mesh resolution (1/6°).

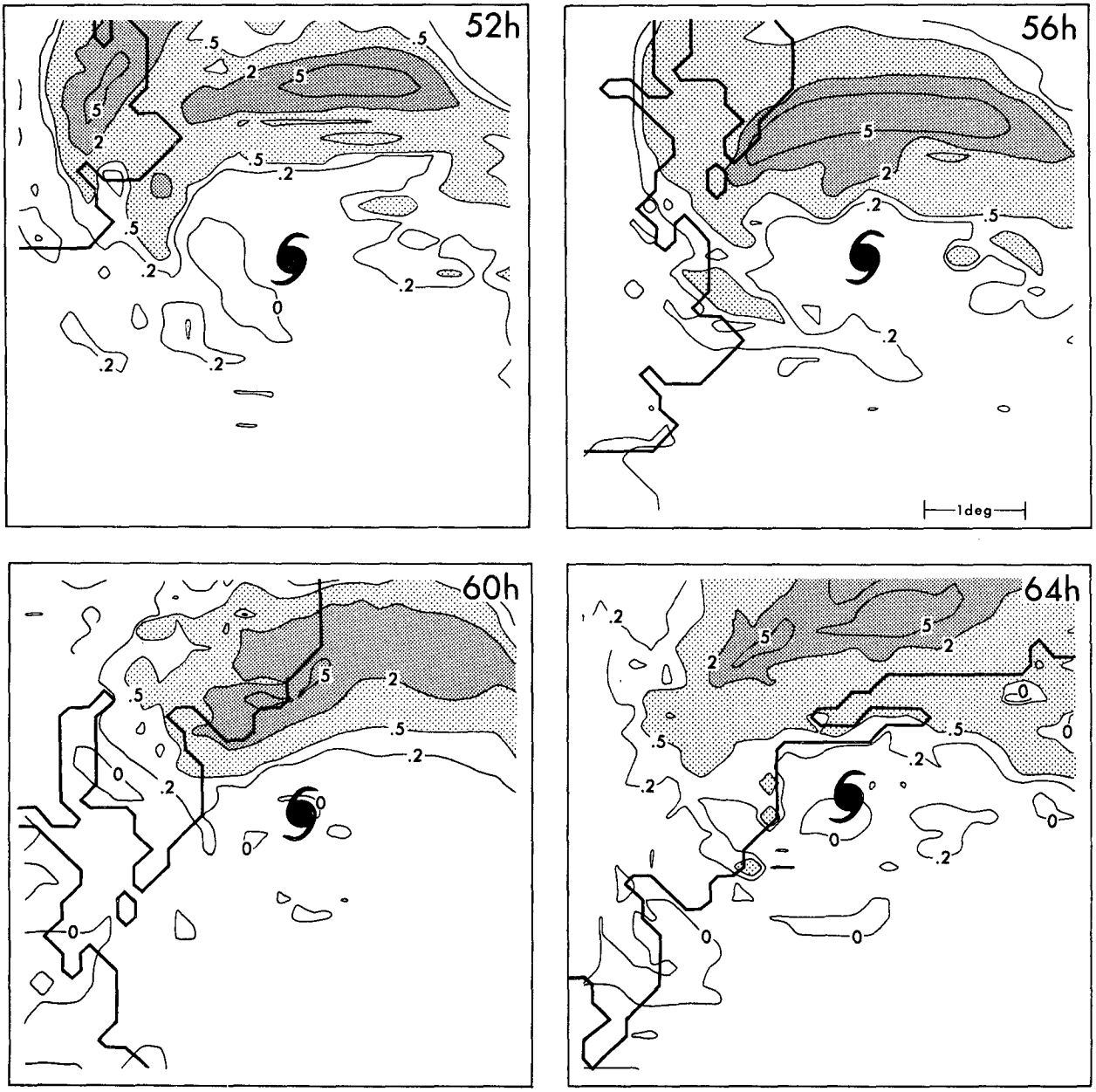

FIG. 5. Rainfall intensity (cm h^{-1}) in the finest mesh area (5° × 5°) for Expt. G25F at 52, 56, 60 and 64 h. Rainfall intensity between 0.5 and 2 cm h^{-1} is lightly shaded with values greater than 2 cm h^{-1} having thicker shading. An additional contour of 5 cm h^{-1} is drawn within the thicker shading. The shoreline plotted is that which is resolved by the finest mesh resolution.

general features of the outer region of the observed hurricane, in particular the absence of significant rain south of the storm and concentration of heaviest rainfall north and northwest of the storm center, appeared to be well reproduced. We speculate that these features were related to the acceleration of the storm. When a vortex propagates with respect to the advection on a long time scale, the required vorticity tendency is obtained primarily from the isallobaric wind. In the planetary boundary layer, this wind, by modifying the primary Ekman-like wind, provides divergence (convergence) and hence a vorticity sink (source) in the back (front) section of the propagating vortex (Young 1973). If the above mentioned boundary layer divergence was a mechanism for the decay of a portion of the eyewall, the structural change of Gloria as well as that of the model storm, was correlated with its accelerated movement. As the model storm approached Long Island, all significant precipitation was found over New England, far north of the storm center.

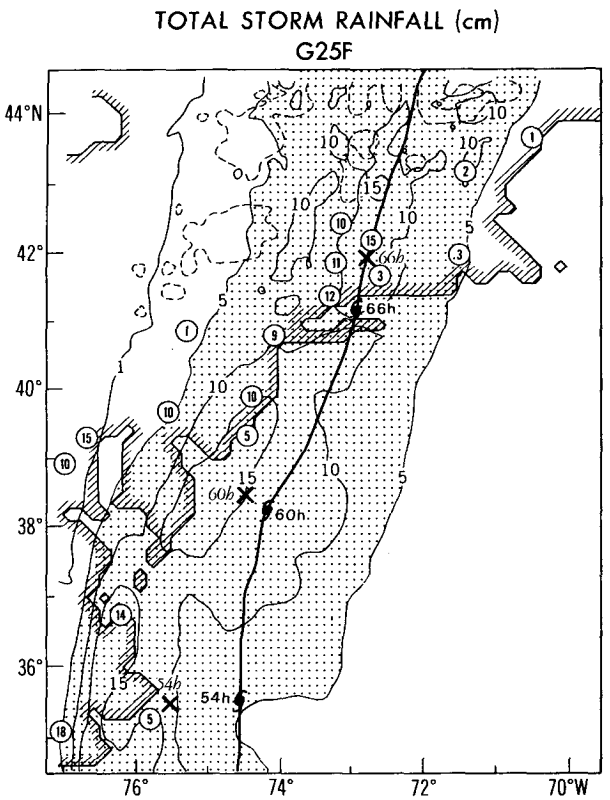

FIG. 6. Distribution of the storm total rainfall (cm, solid line) for Expt. G25F. Total rainfall greater than 5 cm is shaded. The numbers in circles are the observed values (cm) of storm rainfall. See Fig. 4 for more details.

Finally, the distribution of the total storm rainfall during passage of the storm in Expt. G25F is shown in Fig. 6. Since the model storm moved east of the observed track during the period before landfall, the region of heaviest rain was also displaced to the east accounting for underestimates in the amount of rainfall over and to the west of the Chesapeake Bay. After landfall however, the correlation with the observed rainfall amounts appeared quite good. For example, the observations confirmed the forecasted sharp cut off of heavy rainfall at the western and eastern edges of the rainfall swath. Also, locally large rainfall amounts were observed in central New England, which were reproduced by the model. Note that upslope winds, associated with the mountainous topography over central and northern New England, seemed to have enhanced the model predicted precipitation amounts in this region.

4. Results using different boundary datasets

The sensitivity of the model forecast to the specification of the lateral boundary values was tested with two additional integrations which differed from Expt. G25F only in the lateral boundary values used. In Expt. G25A the lateral boundary was forced to values obtained from the T80 analysis and in Expt. G25X the lateral boundary values were forced to the initial values throughout the entire integration. All integrations were run for 72 h using the initial condition previously described.

Orlanski and Katzfey (1987) demonstrated that values specified at the lateral boundaries influenced their limited area model forecast as the integration proceeded, mainly through advection and planetary wave propagation. In their model the southern boundary was placed at 22° or 26°N. Our model domain, which stretched to the equator, included the deep tropics where the constraint of the geostrophic balance becomes weak.

From the storm tracks shown in Fig. 7 we see there was little difference between the 24 h positions of the three experiments. At 48 h, the forecast error for Expt. G25A was 78 km compared to 107 km for Expt. G25F. After 48 h, although neither integration reproduced the degree of observed recurvature, Expt. G25F was more successful than Expt. G25A at predicting the observed storm acceleration. Hence, by 72 h the storm in Expt. G25A was considerably further to the west and south with a forecast error of 342 km, compared with 191 km for Expt. G25F. Although it is somewhat surprising that use of forecast boundary values gave a smaller position error at 72 h compared with the result using analyzed boundary values, this demonstrates the

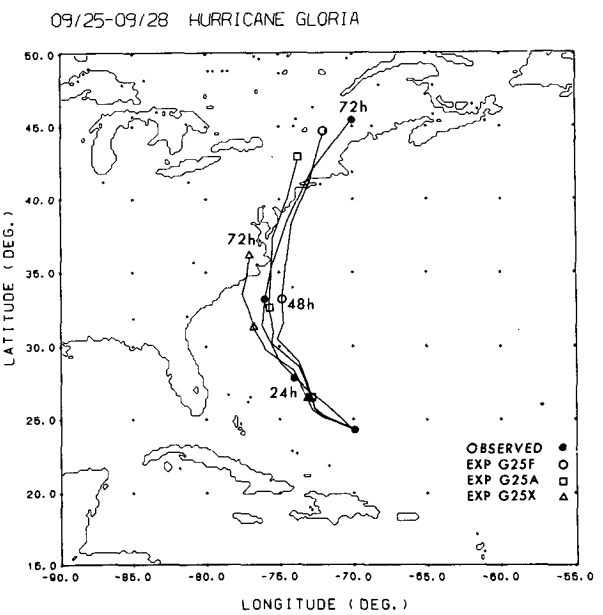

FIG. 7. The 72 h tracks of the storms in Expt. G25F (forecasted boundary condition), Expt. G25A (simulated boundary condition), and Expt. G25X (fixed boundary condition), starting from 0000 UTC 25 September. The observed track (best track) is also plotted for comparison. The marks indicate the daily storm positions valid at 0000 UTC each day.

sensitivity of the storm track to small differences which may evolve in the flow field during the course of the integration. It should be noted that in addition to the influence of the boundary condition, the initial condition as well as the quality of the model also determine the evolution of the flow field. The error originating from the boundary conditions can be masked by the errors due to other sources. Also, the analyzed boundary values may not always be more accurate than the forecast boundary values in the early period of the integration. We also should point out that the success of the 72 h G25F position is partially related to the G25F 48 h position being east of both the observed (best) track and the Expt. G25A position.

The errors originating from the western boundary, if advected by the mean flow, would have reached the storm region at about 36 to 42 h after the initial time. Indeed, when the model was run with the boundary condition fixed to the initial value (Expt. G25X), the position of the storm remained similar to the other two experiments up to about 36 h, after which it began to deviate. By 48 h, the storm in Expt. G25X was located about 240 km south of the observed position. During the last 24 h, the storm center moved slowly in a northward direction at about 6 m s^{-1}, making landfall over North Carolina at about 66 h. Its 72 h position was over 1100 km southwest of the observed position.

The distribution of the total storm rainfall during passage of the storm in Expt. G25A is shown in Fig. 8. Since the storm track was further west of Expt. G25F, and hence better forecasted as the storm passed near Cape Hatteras and Delaware, the total storm rainfall more closely agreed with the observed values in this region. For example, the heavy amounts of rainfall observed over the Chesapeake Bay region and sections of North Carolina were better forecasted compared with Expt. G25F. As the model storm continued moving north, the agreement with the observations began to deteriorate, as the storm moved further west of the observed track.

Although the skill of predicting rainfall and wind speed distributions is dependent on a correct track forecast, it is not assured that a model which reproduces the observed track will also correctly simulate these other fields. Therefore, it is encouraging that our model was successful in reproducing rainfall and wind speed distributions over those regions where the track was well predicted.

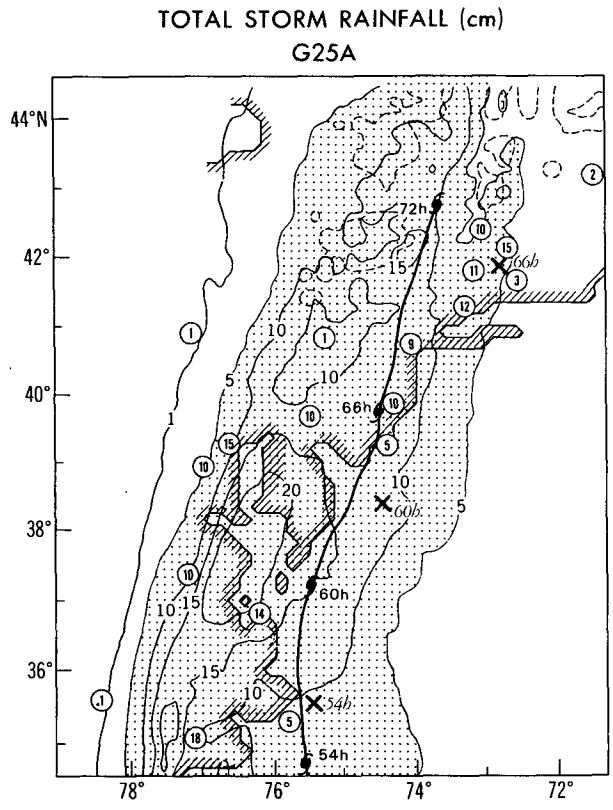

FIG. 8. Distribution of the storm total rainfall (cm, solid line) for Expt. G25A. Total rainfall greater than 5 cm is shaded. The numbers in circles are the observed values (cm) of storm rainfall. See Fig. 4 for more details.

5. Results using coarse resolution models

When a small vortex was traced in a dry model (Kurihara and Bender 1980), the dispersion effect due to the finite differencing contributed more to the deterioration of the vortex structure as the grid resolution became coarser. When moisture was included in the model, however, the vortex could be maintained longer because of the forcing effect due to latent heat release. Since models with coarser resolution than the MMM model are likely to be used, at least for the present at many operational forecast centers, comparison of the forecast results between the coarse resolution models and the MMM model would be useful. Thus, two forecasts with a single nest were made using the same lateral boundary values as Expt. G25F, but with 1° (Expt. G25C) and 1½° (Expt. G25T) resolution throughout the entire domain. The resolution of G25C is the same as the outermost nest of Expt. G25F, while the resolution of the second integration corresponds to the approximate resolution of the T80 spectral model. Both integrations were run to 72 h and compared with Expt. G25F. At 60 h (Fig. 9) the position of all three storms was very similar although the intensity was significantly weaker with the coarser models. For example, the 60 h minimum sea level pressure was 968 mb for Expt. G25F compared to 991 and 996 mb for Expts. G25C and G25T. During the last 12 hours (60 h to 72 h) of the forecast, both storms with the coarser resolution moved more slowly than the storm in Expt. G25F. Thus their position was further to the south by the end of the integration, resulting in a 72 h forecast error of about 340 and 300 km for Expts. G25C and G25T.

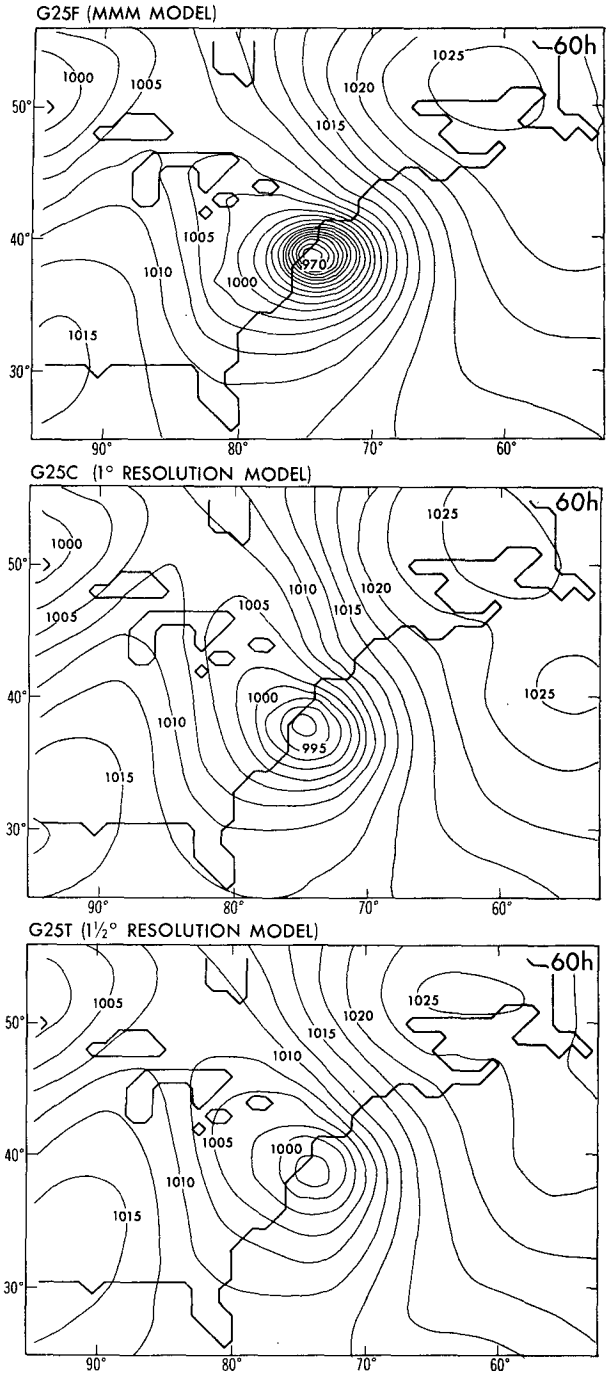

FIG. 9. Distribution of the sea level pressure (mb) for Expt. G25F (top), Expt. G25C (1° resolution experiment, middle), and Expt. G25T (1½° resolution experiment, bottom), at 60 h, for a portion of the integration domain. The shoreline shown is that which is resolved by the 1° model resolution.

It is interesting to note that Expt. G25T, although run with approximately the same resolution as the T80 forecast model, gave a much better forecast than was obtained from the T80 model. By 48 h the storm in the T80 forecast was moving significantly faster than the observed hurricane and was located near the 60 h position of the observed storm. This resulted in a 487 km forecast error at 48 h as shown in Table 4. By 60 h the storm system had almost entirely merged with the extratropical low that was moving across eastern Canada. It is unclear why the GFDL hurricane model, when run with the same resolution as the T80 forecast model, gave a better forecast of the storm track.

Comparison of the rainfall amounts from the coarse resolution experiments with Expt. G25F showed the sensitivity of this quantity to resolution. For example, in Expt. G25C (figure not shown), the maximum rainfall (~14 cm) occurred just off the North Carolina coast with the amounts gradually decreasing to the north, while rainfall along the North Carolina coast was about 10 cm. In contrast, for Expt. G25T, the maximum rainfall (~12 cm) occurred over 150 km east of the North Carolina coast, with values along the coast of North Carolina of only about 4 cm. These amounts compared to values of around 15 cm for Expt. G25F (Fig. 6). Since the rainfall for both of the coarse resolution experiments decreased as the storm moved to the north and accelerated, correlations with the observations were poorest over New England. Here the rainfall for both cases was under 5 cm everywhere, compared to values of locally over 15 cm for Expt. G25F.

Similar to the results for Expt. G25F, the 60 h distribution of the instantaneous precipitation indicated that no precipitation was falling south of the storm center in Expts. G25C and G25T at that time. In Expt. G25C at 60 h, significant precipitation extended from the storm center for about 250 km both to the north and to the east, with maximum rainfall of about 2 cm h^{-1} occurring about 120 km north of the storm center. This was different from the results with the fine mesh resolution (Fig. 5), where no significant precipitation occurred in the regions near the center of the storm itself.

6. Results from extended integrations

In this section, we will present the results of two integrations starting from the 1200 UTC 22 September T80 analysis, 60 hours earlier than the initial conditions of the previous results. The model was integrated 132 hours with boundary conditions taken from either the T80 analysis at 12 hour intervals (Expt. G22A) or an integration of the T80 spectral forecast model (Expt. G22F). The initial position error of the storm center in the T80 analysis on 1200 UTC 22 September was about 130 km. The radius of maximum wind, the minimum sea level pressure, and maximum lowest level winds of the analyzed initial storm were 550 km, 1007 mb, and 29 m s^{-1}. This corresponds to observed values of minimum sea level pressure and maximum lowest level winds of 992 mb and 37 m s^{-1}.

a. Track forecasts

The tracks for both integrations are presented in Fig. 10. The position error at 72 h was 220 km (Expt. G22F) and 380 km (Expt. G22A). This compares with a position error of 580 km and 201 km for the T80 model and the operational MFM forecast model at NMC. The National Hurricane Center's 72 h official track forecast, the NHC83 forecast and the CLIPER forecast from 1200 UTC 22 September had position errors of 514 km, 510 km and 620 km, respectively. It is interesting to note that, similar to Expt. G25F and Expt. G25A, the experiment with forecast boundary values produced a smaller position error at 72 h than that with analyzed boundary values. Most of the error up to 72 h for both boundary conditions resulted from too rapid movement of the storm. This could have partially resulted from the initial vortex size and intensity. Indeed, Fiorino and Elsberry (1989) found that the movement of a nondivergent, barotropic vortex can be influenced by the size of the vortex. After 72 h, the storm in Expt. G22F began to turn toward the northeast and eventually passed far east of the coast. In Expt. G22A, the storm continued to move on a path very close to the observed storm, resulting in a position error of only 73 km after 132 h.

Analysis of the predicted synoptic-scale wind field at 72 h (figure not shown) showed large differences between Expts. G22A and G22F. For example, analysis of the deep layer mean wind for Expt. G22A, as well as the wind field at around 500 mb, indicated that the winds were primarily southwesterly from the western lateral boundary to the eastern portion of the United States. However, the winds over the same region were much more westerly for Expt. G22F. Analysis of the deep layer mean wind also indicated that the southwestern part of the anticyclone over the Atlantic at 72 h was oriented south to north for the case of Expt. G22F. For Expt. G22A, as well as the T80 analyzed field, this feature was oriented more southeast to northwest at this time. This difference apparently resulted in the storm in the two experiments being steered in different directions after 72 h. Since the two experiments differed only in the lateral boundary values used, this demonstrates the importance of high quality boundary conditions for extended periods in the integration of regional models.

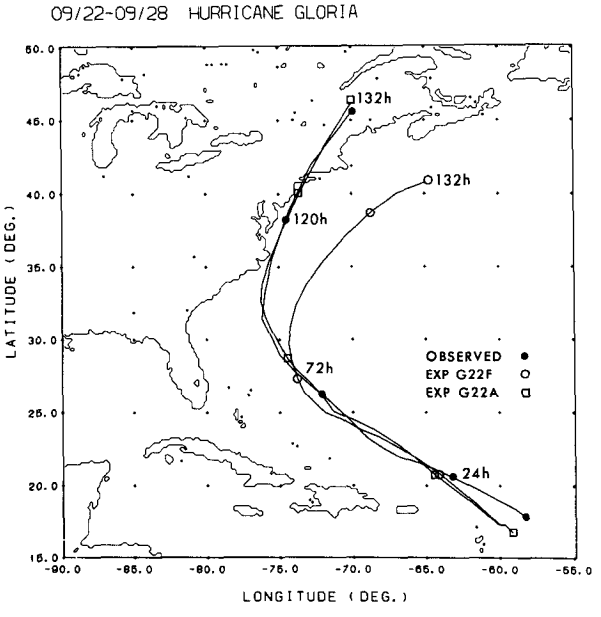

FIG. 10. The 132 h track of the storms in Expt. G22F (forecasted boundary condition) and Expt. G22A (simulated boundary condition), starting from 1200 UTC 22 September. The observed track is also plotted for comparison.

b. Analysis of the storm structure and intensity

Analysis of the structure of the storm in both of the extended integrations showed that the storm evolution differed significantly from the previous integrations. In particular a more intense and much smaller storm evolved. For example, as the storm in Expt. G22A was about one degree latitude south of North Carolina (105 h), the storm's minimum pressure was 959 mb, with low level maximum winds of 42 m s^{-1} and radius of maximum wind of 65 km. In contrast, the storm in Expt. G25F at roughly the same position (50 h) had a minimum surface pressure of 977 mb, maximum surface wind of 27 m s^{-1}, and radius of maximum wind of about 230 km. However, as this storm (Expt. G25F) continued to move up the coast, the minimum pressure decreased to about 967 mb and maximum low level winds increased to slightly greater than 33 m s^{-1} at about the time of landfall. This seems to indicate that the spinup process in G25F was not complete by the time the system began to accelerate up the east coast. In contrast, in Expt. G22A the storm spinup was completed by the time the storm approached the east coast, resulting in a much more realistic storm structure. From Fig. 11 we see that in this simulation, similar to Expt. G25F and the observed case, the eye wall to the south of the storm began to weaken by 109 h as the storm moved north, with most of the significant precipitation occurring north of the storm center. We can also note that the strongest winds were still occurring on the east side of the storm, over the ocean. Likewise, the meridional cross section through the center of the storm (Fig. 12) shows further asymmetric features in the storm structure as well, with the strongest wind at the midlevels of the atmosphere occurring south of the storm center, and in the boundary layer north of the storm. The upward motion is also considerably larger north of the center. As mentioned before, the development of asymmetries in the boundary layer wind field may be associated with the accelerated movement of the storm.

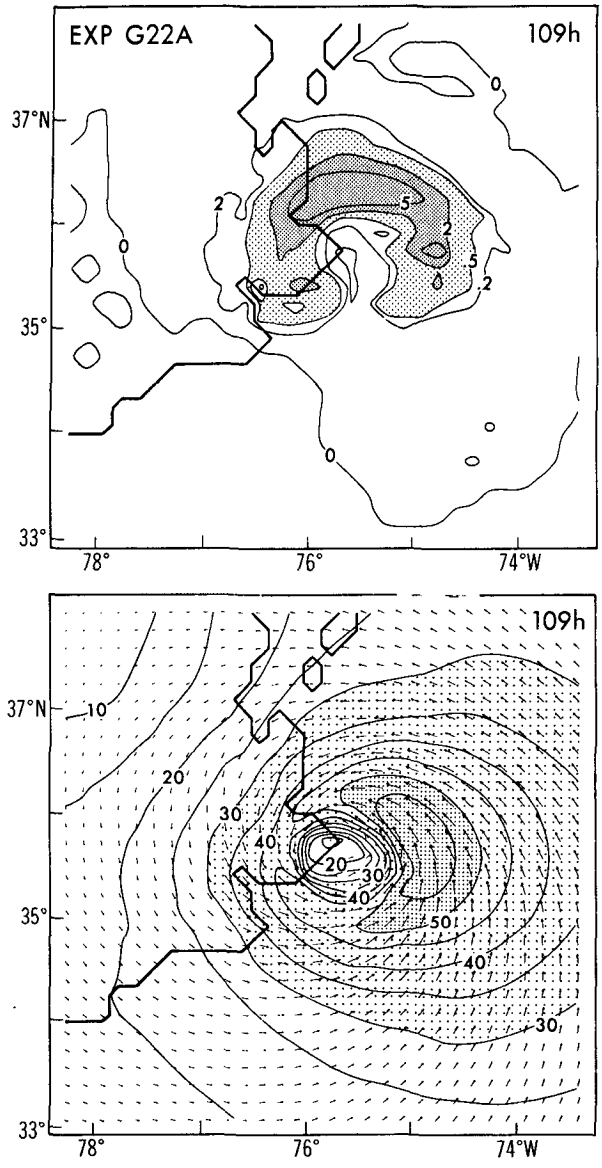

FIG. 11. The distribution of the rainfall intensity (top, cm h^{-1}) and model level 16 ($\sigma = 0.960$) wind speeds (m s^{-1}) and horizontal wind vectors in the finest mesh area for Expt. G22A at 109 h. Rainfall intensity between 0.5 and 2 cm h^{-1} is lightly shaded with values greater than 2 cm h^{-1} having thicker shading. Wind speeds between 30 and 50 m s^{-1} are lightly shaded, with values greater than 50 m s^{-1} having darker shading. The shoreline drawn is that which is resolved by the finest mesh resolution (1/6°).

There was also very good agreement between the observed and the model simulated distribution of maximum low level wind for Expt. G22A (figure not shown), including areas where Expt. G25F failed to reproduce the correct wind speed amounts. For example, the storm in Expt. G22A produced maximum low-level winds slightly in excess of hurricane force along most of the North Carolina coast, in agreement with the observations shown in Fig. 4. As this system progressed up the east coast, the storm continued to gradually weaken (similar to the observed storm) as the radius of maximum wind increased. The minimum surface pressure and maximum low level wind for the model storm at landfall over Long Island were 972 mb and 34 m s^{-1} with a radius of maximum wind about 105 km. In agreement with the observations, strongest winds were still located well to the east of the storm track in Expt. G22A, with maximum winds close to 30 m s^{-1} along parts of the Massachusetts coastline.

Starting from initial times 60 h apart, Expts. G22A and G25F produced vortices which were similar to each other in their overall structural pattern as they rapidly moved north-northeast during 27 September in more or less similar synoptic conditions. However, they differed from each other considerably in their size and intensity. This suggests that some of the gross features in the structure of the storm resulted from the interaction of the vortex with its environment. We anticipate that the forecast of the wind, rainfall, and movement will be improved when the size and intensity of the simulated vortex becomes more realistic. To do so a more intense and realistic vortex will have to be specified initially since the spinup time of the vortex resolved by the NMC analysis is at least two days.

7. Summary and remarks

This study investigated the prediction capability of the GFDL triply-nested, movable mesh regional hur-

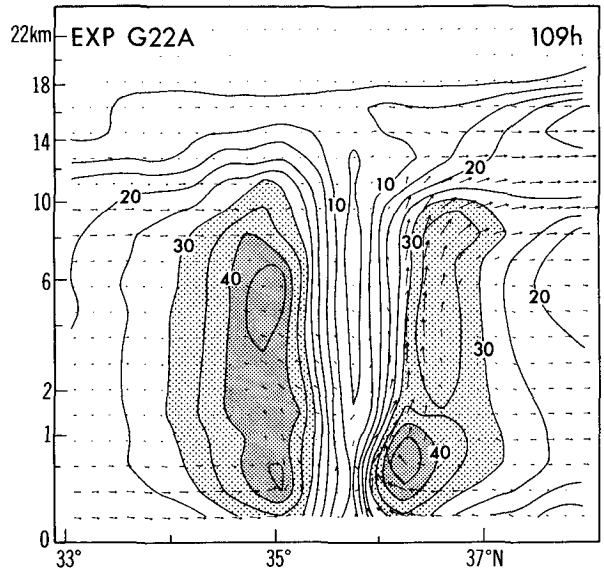

FIG. 12. South–north cross section through the center of the storm (75.75°W) for Expt. G22A, at 109 h. The total wind speed is contoured at 5 m s^{-1} intervals, with values between 30 and 40 m s^{-1} lightly shaded, and values greater than 40 m s^{-1} having darker shading. The arrows show the wind vectors of the meridional and vertical components. The vertical coordinate system is the square root of height in meters (See Fig. 11 of Bender et al. (1985) for more details). The actual height (km) is presented on the left side of the figure.

ricane model for two cases of Hurricane Gloria. We found that the model was able to forecast the significant acceleration of the storm as it recurved up the east coast of the United States. This was in part due to the ability of the model to accurately forecast the evolution of the large scale flow field during the integration of the model when accurate lateral boundary values were specified. The position error of the MMM model was considerably less than that of the NHC official forecast. It was also found that both the model and the observed storm motion closely paralleled the streamlines of the deep layer mean wind field which served as an excellent indicator of the "steering flow" for the storm. A study is under way to examine the utility of the deep layer mean wind in the track prediction of tropical cyclones.

Various 72 h integrations were run with lateral boundary values taken from either an NMC T80 forecast or an NMC T80 global analysis. A supplemental experiment was also run in which the lateral boundary condition remained fixed to the initial value throughout the integration, resulting in a very large forecast error at 72 h. These results showed the sensitivity of the storm track to the type of boundary values specified, especially when the effects of the lateral boundary had propagated into the storm region.

In a set of extended integrations which were started 60 h earlier and were run to 132 h, the effects from the lateral boundary reached the storm region by 72 h. This resulted in a large position error in the storm track after that time for the integration run in forecast mode. The storm track for the integration run in simulation mode remained remarkably close to the observed track, with a position error of only 73 km after 132 hours. This may indicate the potential for accurately forecasting storm track in some cases, when a fine resolution model is used and accurate lateral boundary values can be obtained. Of course, the degree of success will undoubtedly be case dependent, since the accuracy of the lateral boundary dataset is one factor among many which may influence the forecast of the storm track.

For the most part, the track prediction using the MMM model was much improved compared with the T80 forecast. Significant improvements in the forecasted track after 60 h were also obtained, when compared with coarser versions of our limited area model. Although the track up to 60 h was quite similar between the $\frac{1}{6}°$, 1° and $1\frac{1}{2}°$ experiments in the present case, the track error in other cases will probably show more sensitivity to the model resolution and storm intensity than was found in these experiments.

With the increase of resolution from $1\frac{1}{2}°$ to $\frac{1}{6}°$, we found that accurate prediction of other storm quantities such as the asymmetries in the distribution of the low level winds or total storm rainfall during passage of the tropical cyclone were significantly improved. Indeed, it was found that the distributions of these quantities in the MMM model agreed well with the observations when the track was well forecasted. Significant structural changes in Hurricane Gloria, which occurred as the storm accelerated to the north, were reproduced by the model even with the coarser resolutions, at least to a first degree. It appears that some features of the storm's structure were strongly controlled by the interaction of the vortex with its environment and others were more sensitive to the grid resolution.

The proper specification of the initial storm in the model seems to be one of the important factors for the reduction of track forecast error from the initial time to 48 h and beyond. A problem that is currently under investigation and will be addressed in future papers is how to start the integration with a more realistic storm structure and a more accurate storm position and intensity. Since the hurricane vortex in the T80 analysis was much too weak and unrealistically large, a significant amount of spinup time was required after the start of the integration. The integrations which began from the later initial time (0000 UTC 25 September) had not yet completed the spinup process by the time the storm began to accelerate to the north. This resulted in an unrealistic sequence of intensification, in which the model storm continued to deepen to the point of landfall, while the observed storm was actually decaying. This may have resulted in an unrealistically large radius of maximum wind when compared both with observations and with the integrations, which began at an earlier time (1200 UTC 22 September). The problem of appropriately combining the large scale environmental field with the fine scale structure of the storm must be treated very carefully. This may reveal a further potential to improve the prediction of the storm track, structure and intensity.

Acknowledgments. The authors would like to thank J. Mahlman for his continuous support of the hurricane dynamics project at GFDL. They are grateful to E. Kalnay, R. Kistler, and B. Katz of NMC for their cooperation in providing data from the T80 analysis, and for making integrations of their T80 forecast model, used as the host model for all the experiments presented. Without their continuing cooperation, this research would not have been possible. Thanks is also given to M. Lawrence of NHC for supplying us with the CLIPER forecasts presented, to C. Neumann of Science Applications International Corp. and C. McAdie of NHC for providing us with the NHC83 forecast data, and to D. Marks of NMC who supplied the operational MFM forecasts shown. They are grateful to W. Stern of GFDL for providing the programs used to convert the spectral data to grid point data. They would also like to express their appreciation to N. C. Lau and J. Katzfey of GFDL for their valuable comments and criticisms on the original version of this manuscript. Finally, thanks and credit are given to P. Tunison, K. Raphael, J. Varanyak, and J. Conner for preparing the figures.

APPENDIX

Smoothing Operator

Our technique to remove the disturbance from the larger scale field uses successive application of a simple smoothing operator. First, we obtain a field of uniform (1 degree) resolution everywhere by area averaging the data in the fine mesh onto the 1 degree coarse mesh domain. Next, a smoothing operator, similar to that defined by Shuman (1957) is applied to the entire field for each wind component, first in the zonal direction, then in the meridional direction. The smoothing operator is defined as follows:

$$\bar{X}_{i,j} = X_{i,j} + K(X_{i-1,j} + X_{i+1,j} - 2X_{i,j}). \quad \text{(A1)}$$

Here, X denotes the variable being smoothed, $\bar{X}$ the resulting smoothed value, the subscripts i and j refer to points of X equally spaced in the zonal and meridional direction respectively, and K being the smoothing parameter. The above computation is repeated N times, with K, as defined below, varying each time:

$$K = \frac{1}{2}\left(1 - \cos\frac{2\pi}{m}\right)^{-1}. \quad \text{(A2)}$$

In the present case N is 11 and m varies as: 2, 3, 4, 2, 5, 6, 7, 2, 8, 9, 2. (Occasional use of $m = 2$ is done to suppress the negative amplification of possible noise.) Here, sinusoidal waves of wavelength m, defined in units of d (distance between grid points, i.e. 1 degree longitude) will be entirely removed by application of the smoothing operator. The values for the points at the east and west ends remain unchanged during the smoothing in the zonal direction.

Next, the smoothing operator is applied in the meridional direction:

$$\bar{\bar{X}}_{i,j} = \bar{X}_{i,j} + K(\bar{X}_{i,j-1} + \bar{X}_{i,j+1} - 2\bar{X}_{i,j}) \quad \text{(A3)}$$

Again, the above computation is repeated in the same manner as the zonal smoothing. Thus, all waves of length $2d$ to $9d$ are entirely removed from the field. Of course, waves of longer wavelengths are partially damped at each application of the filtering operator. For example, in the final filtered field, waves of length $15d$ will have been damped by 82%, with waves of length $20d$ and $30d$ damped by 60%, and 32%, respectively. The resulting damping profile is similar to the one obtained from repeated application of a two-dimensional nine-point smoothing operator, as proposed by DeMaria (1985). The gradual damping of the longer wavelengths is different from that obtained in some other objective scale separation techniques, in which the damping rate decreases very rapidly beyond a given wavelength (e.g., Maddox 1980). In our method, it is not required to select a particular scale which separates the disturbance from the large scale flow for a given meteorological field.

REFERENCES

Akima, H., 1978: A method of bivariate interpolation and smooth surface fitting for irregularly distributed data points. *ACM Trans. Math. Software,* **4**(2), 148–159.

Bender, M. A., R. E. Tuleya and Y. Kurihara, 1985: A numerical study of the effect of a mountain range on a landfalling tropical cyclone. *Mon. Wea. Rev.,* **113,** 567–582.

——, —— and ——, 1987: A numerical study of the effect of island terrain on tropical cyclones. *Mon. Wea. Rev.,* **115,** 130–155.

Case, R. A., 1986: Atlantic hurricane season of 1985. *Mon. Wea. Rev.,* **114,** 1390–1405.

Dell'Osso, L., and L. Bengtsson, 1985: Prediction of a typhoon using a fine mesh NWP model. *Tellus,* **37A,** 97–105.

DeMaria, M., 1985: Tropical cyclone motion in a nondivergent barotropic model. *Mon. Wea. Rev.,* **113,** 1199–1210.

Fiorino, M., and R. L. Elsberry, 1989: Some aspects of vortex structure related to tropical cyclone motion. *J. Atmos. Sci.,* **46,** 975–990.

Franklin, J. L., S. J. Lord and F. D. Marks, 1988: Dropwindsonde and radar observations of the eye of Hurricane Gloria (1985). *Mon. Wea. Rev.,* **116,** 1237–1244.

Heckley, W. A., M. J. Miles and A. K. Betts, 1987: An example of hurricane tracking and forecasting with a global analysis-forecasting system. *Bull. Amer. Meteor. Soc.,* **68,** 226–229.

Iwasaki, T., H. Nakano and M. Sugi, 1987: The performance of a typhoon prediction model with cumulus parameterization. *J. Meteor. Soc. Japan,* **65,** 555–570.

Krishnamurti, T. N., and D. Oosterhof, 1989: Prediction of the life cycle of a supertyphoon with a high-resolution global model. *Bull. Amer. Meteor. Soc.,* **70,** 1218–1230.

——, —— and N. Dignon, 1989: Hurricane prediction with a high resolution global model. *Mon. Wea. Rev.,* **117,** 631–669.

Kurihara, Y., 1973: A scheme of moist convective adjustment. *Mon. Wea. Rev.,* **101,** 547–553.

——, and M. A. Bender, 1980: Use of a movable nested mesh model for tracking a small vortex. *Mon. Wea. Rev.,* **108,** 1792–1809.

——, C. L. Kerr and M. A. Bender, 1989: An improved numerical scheme to treat the open lateral boundary of a regional model. *Mon. Wea. Rev.,* **117,** 2714–2722.

Maddox, R. A., 1980: An objective technique for separating macroscale and mesoscale features in meteorological data. *Mon. Wea. Rev.,* **108,** 1108–1121.

Mellor, G. L., and T. Yamada, 1974: A hierarchy of turbulence closure models for planetary boundary layers. *J. Atmos. Sci.,* **31,** 1791–1806.

Neumann, C. J., 1979: On the use of deep-layer-mean geopotential height fields in statistical prediction of tropical cyclone motion. *Sixth Conf. on Probability and Statistics in Atmospheric Sciences,* Banff, Amer. Meteor. Soc., 32–38.

——, 1988: The National Hurricane Center NHC83 Model. NOAA Tech. Memo. NWS NHC 41, Natl. Hurricane Center, Coral Gables, Florida, 44 pp.

——, and J. M. Pelissier, 1981: Models for the prediction of tropical cyclone motion over the North Atlantic: An operational evaluation. *Mon. Wea. Rev.,* **109,** 522–538.

Orlanski, I., and J. J. Katzfey, 1987: Sensitivity of model simulations for a coastal cyclone. *Mon. Wea. Rev.,* **115,** 2792–2821.

Powell, M. D., 1982: The transition of the Hurricane Frederic boundary-layer wind fields from the open Gulf of Mexico to landfall. *Mon. Wea. Rev.,* **110,** 1912–1932.

Sanders, F., and R. W. Burpee, 1968: Experiments in barotropic hurricane track forecasting. *J. Appl. Meteor.,* **7,** 313–323.

Shuman, F. G., 1957: Numerical methods in weather prediction: II. Smoothing and filtering. *Mon. Wea. Rev.,* **85,** 357–361.

Tuleya, R. E., M. A. Bender and Y. Kurihara, 1984: A simulation study of the landfall of tropical cyclones using a movable nested-grid model. *Mon. Wea. Rev.,* **112,** 124–136.

Young, J. A., 1973: A theory for isallobaric air flow in the planetary boundary layer. *J. Atmos. Sci.,* **20,** 1584–1592.